International Journal of Thermal Sciences 48 (2009) 1043–1048

Contents lists available at ScienceDirect

International Journal of Thermal Sciences

www.elsevier.com/locate/ijts

Buoyancy-driven convective motion in a thermal diffusion cloud chamber using a water/helium mixture

Françoise Utheza [a,*], Dorothée Sénechal [a], François Garnier [b]

[a] Université de Marne-la-Vallée, LETEM, Bât. Lavoisier, Champs-sur-Marne, 77454 Marne-la-Vallée Cedex 02, France
[b] Office National d'Etudes et de Recherches Aérospatiales, 29 avenue de la division Leclerc, 92320 Châtillon, France

ARTICLE INFO

Article history:
Received 4 May 2005
Received in revised form 9 March 2007
Accepted 28 September 2008
Available online 26 January 2009

Keywords:
Numerical simulation
Thermal diffusion cloud chamber
Water/helium mixture
Conductive/convective regime
Homogeneous nucleation
Supersaturation

ABSTRACT

This work is focused on a 2D numerical simulation of a thermal diffusion cloud chamber (TDCC) operating with water–helium mixture. We particularly address the impact of the stability of the vapor–gas mixture with respect to buoyancy-driven convective motion on homogeneous water nucleation rates. A comparison of our model results with Heist and Reiss results of nucleation of water in helium is first proposed. So, no convective fluxes are assumed within the TDCC and the critical supersaturation of water vapor is in agreement as obtained from numerical predictions. However, the influence of wall heating on the critical supersaturation results is found to be significant as obtained when convective transfers is accounted for within the TDCC and the results deviate significantly from those provided by Heist and Reiss. Their approach may lead large differences in terms of temperature, saturation ratio and nucleation profiles as it oversimplifies heat and mass transfer in TDCC compared to a 2D mass, heat and momentum model.

Published by Elsevier Masson SAS.

1. Introduction

The formation of liquid droplet from water vapor is an area of intense efforts because of practical importance in many chemical engineering operations and meteorological applications. This process has been well studied for a long time [1–7] and although great progress has been made in understanding of homogeneous nucleation in water vapor, there is still a number of open questions about the validity of theoretical approaches of the nucleation phenomenon.

Experimental studies use either an adiabatic expansion device (piston cloud chamber, supersonic nozzle…) or a stationary operating system: the thermal diffusion cloud chamber (TDCC) to produce a critical supersaturation state in the apparatus. It was clear from these studies that the main parameters controlling the kinetics of homogeneous nucleation are temperature and vapor concentration (or the corresponding saturation ratio). However, most theoretical studies are not able to predict with acceptable confidence the experimental observations.

One possible cause for the disagreement noted between observations and theory may lie in the interpretation of the experimental data and an important issue, which has been addressed in the past 10 years, concerns the stability of the vapor–gas mixture in a TDCC with respect to buoyancy-driven convective motion, since it may finally yield a misleading rendering of the experimental results. Indeed, Heist et al. [8,9] have shown that the presence of a non-condensable component (carrier gas) influences the clustering process, that the use of heavy carrier gases in a TDCC may influence the stable stratification of the vapor gas mixture with the non-condensable gas and may therefore lead to convection. Moreover, the heated chamber wall (the wall is heated to be kept clean of condensate) may cause a buoyancy driven convection that can propagate towards the center of the chamber and cause a motion of the gas mixture (Ferguson and Nuth [10]). These effects have been examined numerically by Schaeffer et al. [11] who used a 2D mass, heat and momentum numerical model to show that the choice of the carrier gas within the TDCC is of importance since an inappropriate choice can alter the nucleation processes. Quite recently, Ferguson et al. [12] performed a similar analysis with lower molecular weight gases and with an emphasis on the effect of the total pressure on the TDCC operation. Another 2D model of coupled mass, heat and momentum transport in TDCC has been developed by Stratmann et al. [13] taking into account the effects of wall heating, total chamber pressure, carrier gas and chamber geometry on nucleation rates.

The objective of the present study is to continue these modelling efforts concerning the stability in a TDCC. For this, we will re-examine the experiments performed by Heist and Reiss [4] on the nucleation of water vapor. It will be shown that their operating conditions may lead to an alteration of the stable stratification in

* Corresponding author. Tel.: +33 1 60 95 73 08; fax: +33 1 60 95 72 94.
E-mail addresses: utheza@univ-mlv.fr (F. Utheza), francois.garnier@onera.fr (F. Garnier).

1290-0729/$ – see front matter Published by Elsevier Masson SAS.
doi:10.1016/j.ijthermalsci.2008.09.005

Nomenclature

C_p	specific heat at constant pressure	$J\,kg^{-1}\,K^{-1}$	
D	coefficient of the diffusion	$m\,s^{-2}$	
g	gravitational acceleration	$m\,s^{-2}$	
H	height of the chamber	m	
k	Boltzmann constant	$J\,K^{-1}$	
k_s	thermal conductivity	$W\,m^{-1}\,K^{-1}$	
J	nucleation rate droplet number	$m^{-3}\,s^{-1}$	
L	width of the chamber	m	
Le	Lewis number		
L_v	latent heat of evaporation	$J\,kg^{-1}$	
M	molecular weight	$kg\,mol^{-1}\,K^{-1}$	
$\dot{M}$	rate of condensed mater	$kg\,m^{-3}\,s^{-1}$	
N	ratio of thermal and mass buoyancy		
N_a	Avogadro constant	mol^{-1}	
P	pressure	Pa	
P_p	partial pressure	Pa	
P_{sat}	saturation pressure of water	Pa	
Pr	Prandtl number		
P_{tot}	total pressure	Pa	
q	heat flux	J	
Ra_M	solutal Rayleigh number ($Ra_M = g\beta_M \Delta W l^3/\nu D$)		
Ra_T	thermal Rayleigh number ($Ra_T = g\beta_T \Delta T l^3/\nu\alpha$)		
r_p	droplet radius	m	
S	supersaturation ($S = P_v/P_{sat}$)		
S_{ur}	surface	m^2	
T	temperature	K	
U	velocity	$m^2\,s^{-1}$	
W	mass fraction		

Greek symbols

α	thermal diffusivity	$m^2\,s^{-1}$
α_c	condensation coefficient	
β_M	solutal expansion coefficient	
β_T	thermal expansion coefficient	K^{-1}
ν	cinematic viscosity	$m^2\,s^{-1}$
ρ	density	$kg\,m^{-3}$
σ	surface tension	$J\,m^{-2}$
$\Delta\tilde{G}$	Gibbs free energy	J
ΔT	characteristic temperature difference $T_{lower} - T_{upper}$	
ΔW	characteristic mass fraction difference $W_{lower} - W_{upper}$	

Subscripts, superscripts

l	liquid (water)
g	background gas (helium)
v	vapor (water)
$*$	dimensionless
o	reference

the TDCC. A comparison between our numerical work, Heist and Reiss results, and the empirical correlation described recently by Wölk et al. [7] will be made, in order to calculate a corrected nucleation rate.

2. Theoretical method

2.1. Governing equations

We address these open questions using numerical resolution of two sets of equations, a simplified one based on a 2D model of mass and heat transport (pure diffusion simulation, not detailed in the present work), similar to this used by Stratmann et al. [13], and the Navier–Stokes equations in order to describe the mass, momentum and heat transfers in the TDCC. In the latter case, the continuity, momentum and energy equations as well as the conservation of vapor mass are written assuming steady state and thermodynamic equilibrium. In addition, the Soret and Dufour effects are neglected and it is also assumed that the vapor is a dilute species. Finally the vapor and the background gas are assumed to behave a perfect gas.

Based on the Boussinesq approximation, the following assumptions are introduced:

(1) The density ρ_0 of the mixture is assumed to be constant except in the buoyancy term where it is as a linear function of temperature and mass fraction.
(2) All other fluid properties are assumed constant.

Note that relatively large density and temperature gradients occur within the TDCC, consequently the constant property models are not completely acceptable, but may be adequate to predict qualitative behavior. Furthermore among the constant property models, the one based on the arithmetic average temperature shows the best performance (see [14] for instance).

Finally, the problem to solve is described by the following system of 2D-cartesian:

dimensionless equations:

- continuity equation:

$$\nabla.\mathbf{U}^* = 0 \tag{1}$$

- momentum equation:

$$\nabla(\mathbf{U}^*.\mathbf{U}^*) = -\nabla P^* + Pr\nabla^2\mathbf{U}^* + Ra_T Pr(T^* + NW^*)\mathbf{k} \tag{2}$$

- energy equation:

$$\nabla.(T^*\mathbf{U}^*) = \frac{\Delta\omega}{Le}\frac{(C_{pv} - C_{pg})}{C_{p0}}\nabla.(T^*\nabla W^*) + \nabla^2 T^* + \dot{M}^* L_v^* \tag{3}$$

- vapor conservation equation:

$$\nabla.(W^*\mathbf{U}^*) = \frac{1}{Le}\nabla.(\nabla W^*) - \dot{M}^* \tag{4}$$

where $\mathbf{U}^*$, P^*, T^* and W^* are respectively the dimensionless gas velocity, kinematic pressure, temperature and mass fraction given by the following expressions:

$$\mathbf{U}^* = \frac{\mathbf{U}H}{\alpha}, \qquad P^* = \frac{H^2}{\rho_0\alpha^2}P, \qquad T^* = \frac{T - T_0}{\Delta T}$$

$$W^* = \frac{\omega_v - \omega_0}{\Delta\omega}, \qquad \dot{M}^* = \frac{\dot{M}H^2}{\rho_0\alpha\Delta\omega}, \qquad L_v^* = \frac{L_v\Delta\omega}{C_{p0}\Delta T}$$

with ρ_0 the density at the temperature T_0 ($T_0 = (T_{upper} + T_{lower})/2$) and C_{p0} the specific heat at constant pressure of the background gas at the temperature T_0. $\Delta\omega = \omega_{lower} - \omega_{upper}$ denotes the characteristic mass differences. N is a measure of the relative importance of buoyancy forces induced by temperature or mass difference; it is defined as:

$$N = \beta_M\Delta\omega/(\beta_T\Delta T) = Ra_M/(Ra_T Le) \tag{5}$$

The thermal Rayleigh number Ra_T depends on the properties of the carrying gas and on the geometrical dimensions of the TDCC and compares the relative importance of the buoyancy forces with the viscous forces.

$$Ra_T = \frac{g\beta_T \Delta T H^3}{\nu\alpha} \tag{6}$$

where g is the gravitational acceleration, β_T the thermal expansion coefficient

$$\beta_T = -\frac{1}{\rho_0}\frac{\partial\rho}{\partial T}\bigg|_{\omega_0, P_0} \tag{7}$$

ΔT denotes the characteristic temperature differences ($\Delta T = T_{\text{low}} - T_{\text{up}}$), H the height of the TDCC, ν is the viscosity of the mixture and α the thermal diffusivity. The solutal Rayleigh number is given by:

$$Ra_M = \frac{g\rho_0\beta_M H^3 \Delta\omega}{\mu D_{gv}} \tag{8}$$

where D_{gv} is the binary diffusion coefficient. β_M refers to the solutal expansion coefficient

$$\beta_M = -\frac{1}{\rho_0}\frac{\partial\rho}{\partial\omega}\bigg|_{T_0, P_0} \tag{9}$$

The third term in the right-hand side of Eq. (3) is the contribution of phase change to the energy variation, $\dot{M}$ being the dimensionless rate of condensed mater. This rate is calculated using the nucleation rate defined below and the cluster radius from the nucleation theory. Since the number of droplets formed is low and their radius is small, the rate of condensing vapor within the cloud chamber is negligible in comparison with the amount of liquid formed at the upper plate. Moreover, since a cloud chamber is an enclosure working in steady state conditions, the amount of liquid formed at the upper plate is re-evaporated at the lower plate.

The nucleation rate is calculated using the classical Becker–Döring–Zeldovitch theory of homogeneous nucleation [15]. The homogeneous rate J can be specified as:

$$J = B\exp(-\Delta\tilde{G}/kT) \tag{10}$$

where $\Delta\tilde{G}$ is the Gibbs free energy of cluster formation, i.e. the elevation of the free energy required for a transition from a monomer to a cluster. B, first calculated by Becker and Döring [15], is a function of the fluid properties, equilibrium vapor pressure P_e, temperature and supersaturation S. The nucleation rate is dominated by the free energy of cluster formation given by the expression:

$$\Delta\tilde{G} = \frac{4}{3}\pi r_p^2 \sigma \tag{11}$$

where σ is the surface tension, and r_p is the radius of the cluster formed which is a function of fluid properties, temperature and supersaturation. The supersaturation is defined as the ratio between the actual vapor partial pressure and the saturation vapor pressure (or equilibrium vapor pressure at the same temperature).

2.2. Cloud chamber description

A cross-sectional sketch of a typical thermal diffusion cloud chamber is shown in Fig. 1. The cloud chamber consists of a hot lower plate and a cold upper plate. The inside width of the chamber is denoted by L and its height is H. The bottom plate is covered with a thin film of the liquid to be studied and the whole chamber is filled with a non-condensing, non-reacting carrier gas. The amount of carrier gas in the chamber determines the total pressure. The liquid vaporizes on the bottom plate and migrates through the chamber towards the upper plate where it condenses. The top of the chamber is gently sloping to prevent the liquid formed on it falling through the chamber. Thus the liquid flows along the side wall down to the film on the bottom. Under appropriate supersaturation conditions, droplets can form at about three-quarters of the total height [16].

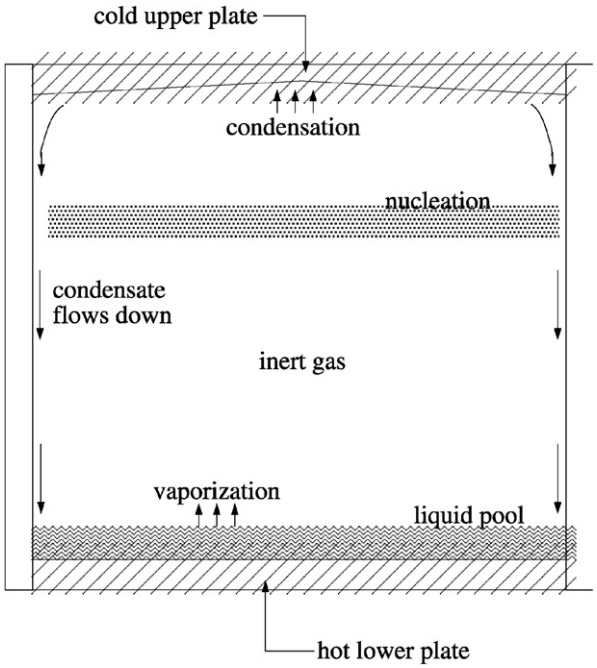

Fig. 1. Cross-sectional diagram of a typical thermal diffusion cloud chamber.

Table 1
Expression for molecular weight M, surface tension σ, mass density ρ, saturation vapor pressure P_{sat}, thermal conductivity λ, dynamic viscosity μ, binary diffusion coefficient D_{ab} and the binary diffusion coefficient temperature dependence, mass heat capacity at constant pressure C_p in S.I. units.

Water:
$M = 18.015$
$\sigma = (93.6635 + 0.009133T - 0.000275T^2)\cdot 10^{-3}$
$\rho = 1000 - 1000((T - 277.1363)^2(T + 15.7914)/508929.2(T - 205.02037))$
$\text{Log}_{10}(P_{\text{sat}}/133.322) = 19.301 - (2892.369/T) - 2.893\,\text{Log}_{10}(T) - 4.937\cdot 10^{-3} * T + 5.607\cdot 10^{-6} * T^2 - 4.646\cdot 10^{-9} * T^3 + 3.787\cdot 10^{-12} * T^4$
$\lambda = (-1.6487\cdot 10^{-5} + 1.9895\cdot 10^{-7} * T) * 4.18\cdot 10^2$
$\mu = 183.5\cdot 10^{-8}[T^{1.5}/(T + 668.3)]$
$C_p = 1.859.25$
Helium:
$M = 4.0026$
$\rho = 0.1895 - 5.098.10^{-4}(T - 273.15) + 4.877\cdot 10^{-7}(T - 273.15)^2$
$D_{ab} = 0.719,\ s = 0.75$
$\lambda = (7.376974\cdot 10^{-5} + 1.139222\cdot 10^{-6} * T - 6.343536\cdot 10^{-10} * T^2) * 4.18\cdot 10^2$
$\mu = 145.5\cdot 10^{-8}[T^{1.5}/(T + 74.1)]$
$C_p = 5.19\cdot 10^3$

The physical property data for water and helium used in this analysis is identified in Table 1.

2.3. Numerical method and boundary conditions

The governing equations are solved numerically using a control volume method and the SIMPLER algorithm [17] for the velocity-pressure coupling. All of the numerical simulations discussed here are performed on a 80×50 regular grid. Steady-state condition was considered to be reached when the following convergence criterion was satisfied

$$\varepsilon = \varepsilon_T + \varepsilon_\omega + \varepsilon_v \tag{12}$$

with

$$\varepsilon_x = \sqrt{\frac{\sum_{\mathrm{IMAX}\times\mathrm{JMAX}}(x - x_{\mathrm{old}})^2}{\mathrm{IMAX}\times\mathrm{JMAX}}} \tag{13}$$

where x denotes temperature, mass fraction and norm of the velocity vector. IMAX and JMAX are the number of nodes in the two directions of the grid and x_{old} is the value of x at the previous calculation step. In the present study, the ε-value was kept to 10^{-5}.

The initial and boundary conditions used for this work are defined as follows. At the upper and lower plates, the temperatures and the mass fraction were kept uniform and constant. Although these two plates are covered with a liquid pool of the condensable species, it is assumed that the velocity components are zero because the liquid layer is so thin that the velocities at the interface can be neglected [10]. Indeed the calculation of evaporating velocity at the lower plate leads to the value of $1.4 \cdot 10^{-3}$ mm/s.

In their works, Heist and Reiss specify that heating imposed on the Pyrex side walls lies between 50 and 60 W. To model side heating, a horizontal temperature gradient is imposed on the vertical walls of the chamber.

The heat balance on the side wall is written:

$$-k_s S_{\mathrm{ur}}\left(\frac{\partial T}{\partial x}\right) = q_{\mathrm{exp}} \tag{14}$$

Thus the expression of the non-dimensional heat flux is:

$$\left[\frac{\partial T^*}{\partial x^*}\right]_{x^*=0} = -q^* = -\left(\frac{q_{\mathrm{exp}}}{k_s \Delta T}\right) \tag{15}$$

The thermal conductivity will be taken equal to $k_s = 1.3$ W/(m K).

3. Results

As already explained in the introduction, this work is focused on a comparison of the model results with the theoretical and experimental data of nucleation of water in helium reported by Heist and Reiss [4]. Note that because of the supersaturated vapor within the TDCC, it is practically impossible to determine the local profiles in terms of temperature, saturation ratio and nucleation by direct measurements and they have to be provided using an acceptable model of transport process. As currently performed in this kind of work, a 1D model of mass and heat transport has been used by Heist and Reiss.

The results (see Fig. 3 in [4]) obtained for a rate of nucleation $J \approx 1$ cm^{-3} s^{-1} include the maximum saturation ratio with respect to the temperatures imposed between the upper and the lower plates and the total pressure in the chamber.

3.1. Numerical results in the conductive regime

A first simulation was performed assuming that there is no convection within the TDCC and that heat and mass transfer occur by diffusion only (i.e. conductive regime). We have reported in Fig. 2 the critical supersaturation data with respect to the temperature, as originally shown by Heist and Reiss [4] (thin line). The critical supersaturation of water vapor as obtained from numerical predictions is in good agreement with state-of-art 1D model results and with experimental data provided by a TDCC operating with a water/helium mixture (see Table 2). As a validation, our 2D model (neglecting convective fluxes and wall heating) is able to properly describe the 1D modeling of mass and heat transport process performed by Heist and Reiss.

We have also incorporated in Fig. 2 (thick line) the values predicted using the Becker–Döring theory (see Eq. (10)) and the numerical results calculated by using the heat and mass equations (dashed line). The prediction of classical nucleation theory

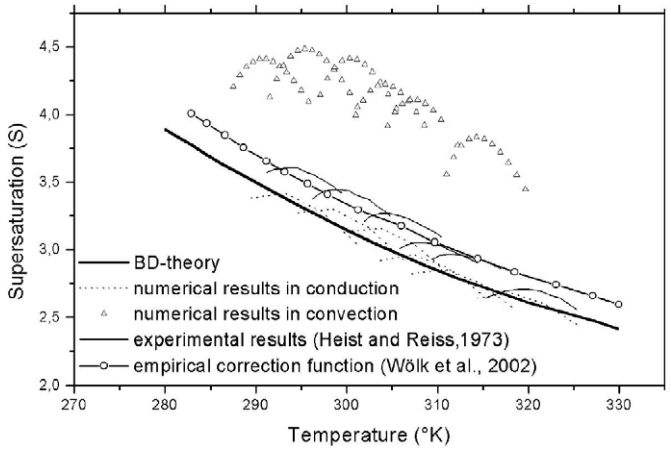

Fig. 2. The variation of the critical supersaturation of water vapor as a function of temperature. The thick line is the saturation predicted by the Becker–Doëring–Zeldovitch theory. The thin lines denote experimental data as reported by Heist and Reiss [4]. The line–white circles represent the corrected saturation provided by Wölk et al. [7]. The dash lines represent the numerical results in conductive regime (i.e. no convective fluxes within the TDCC). The triangles predict the critical supersaturation when the convective flow is accounted for in the modelling.

Table 2
Comparison of maximum saturations obtained from experiments and numerical calculations in conductive regime for water in helium.

	Total pressure in mm Hg	Lower plate temperature in K	Upper plate temperature in K	*Pr*	*Sc*	Experimental maximum saturation	Numerical maximum saturation
Exp 1	737.7	341.59	280.07	0.703	1.025	3.59	3.43
Exp 2	768.6	346.91	285.23	0.701	1.163	3.44	3.33
Exp 3	728.4	351.73	290.63	0.701	1.26	3.26	3.13
Exp 4	729.6	354.67	294.64	0.701	1.29	3.05	2.95
Exp 5	757.7	358.05	298.02	0.702	1.366	2.96	2.86
Exp 6	753.6	364.57	305.33	0.703	1.39	2.70	2.56

for H_2O in the temperature range 280–330 K is known to be incorrect and the theoretical values of critical saturation are observed to be about 8% lower than the results reported by Heist and Reiss in their work. This discrepancy between experimental and theoretical data has recently conducted Wölk et al. [7] to suggest a correction function of the theoretical nucleation rate of Becker–Döring–Zeldovitch.

These authors have developed an empirical correction of the expression of the nucleation rate of the following form:

$$J^{\mathrm{corr}} = J \exp\left(A + \frac{B}{kT}\right) \tag{16}$$

$$J^{\mathrm{corr}} = \left[\frac{\alpha_c}{\rho_l}\left(\frac{2N_a^3 M_l \sigma_l}{\pi}\right)^{1/2} S\left(\frac{P_{v,\mathrm{sat}}}{RT}\right)^2 \exp\left(-\frac{\Delta \tilde{G}}{kT}\right)\right] \times \exp\left(A + \frac{B}{kT}\right) \tag{17}$$

with $A = -27.56$ and $B = 6.5 \times 10^3$.

Since the nucleation rate is a function of saturation, one can deduce that:

$$S^{\mathrm{corr}} = \exp\left[|\ln S| \frac{1}{\sqrt{1 + (M/G)(\ln S)^2}}\right] \tag{18}$$

$$\text{with} \quad M = \left(A + \frac{B}{kT}\right) \tag{19}$$

Other simulations have been performed involving the corrected nucleation rate in order to obtain a new curve of supersaturation vs temperature that corresponds to the individual experiments and

Table 3
Rayleigh numbers, Lewis number and buoyancy ratio for the simulation of water in helium in a TDCC.

	Ra_T	Ra_M	Le	N
Exp 1	5868	−8880	1.35	−1.12
Exp 2	5456	−10480	1.40	−1.37
Exp 3	5046	−10562	1.16	−1.79
Exp 4	4690	−12993	1.32	−2.08
Exp 5	4531	−14284	1.37	−2.29
Exp 6	4091	−16904	1.36	−3.03

a nucleation rate of $J = 1\ \mathrm{cm}^{-3}\,\mathrm{s}^{-1}$. As observed by the authors this correction provides a substantial improvement over the classical theory as shown in Fig. 2 when the results are represented by the open circles.

3.2. Numerical results in the convective regime

A series of cases was run to demonstrate the role of convective flows within the chamber on the maximum saturation with respect to the temperature. In these cases, the momentum equation is used to solve the velocity fields inside the TDCC. The following discussion outlines the difference between the two approaches (i.e. conductive and convective regimes) to emphasize the importance of vapor transport which may exhibit a complex motion within the TDCC.

The fluid motion by natural convection is due to the temperature variation imposed between the two horizontal plates. The decrease of the density of a gas or a liquid when the temperature increases creates an upward flow of the fluid in contact of the hot wall. When the temperature decreases, the density of the fluid increases and a downward movement appears at the contact with the cold wall. Natural convection is characterized by the Rayleigh–Bénard cells which represent the fluid motion under the effect of the density gradient.

To outline the relative importance of these physical phenomena it is convenient to introduce. The thermal Rayleigh number in the case of the experiments carried out by Heist and Reiss [4], it varies from 4000 to 6000 (see Table 3). It corresponds to a natural convection regime. Nevertheless, since the molecular weight of water vapor is higher than that of helium, the concentration expansion coefficient is negative and thus the solutal Rayleigh number is always negative (Table 3), so that thermal and solutal buoyancy effects are opposite. For $Le = 1$, the buoyancy effects cancel; convection disappears and the mass and heat transfers are diffusion dominated [18].

However the temperature and supersaturation profiles along the vertical centerlines are no longer linear as displayed in Fig. 3 and the isotherms (see Fig. 4a) have a sinusoidal shape. Indeed the chamber wall overheating affects the temperature profile in the center portion of the cloud chamber [19] and causes a buoyancy driven convection that can propagate towards the center of the chamber leading to the motion of the gas mixture [13]: roll-shaped cells can be observed in the TDCC and the inert gas is then mixed (Fig. 4d). Note that, in the case of the study performed by Heist and Reiss [4], the two horizontal boundary plates were circular. The pattern of circular rolls arranged in a such geometry is similar to those observed in a rectangular chamber, i.e. with a periodicity in one of the directions but without angular periodicity [20]. However irregular roll patterns can be observed in a cylindrical container: the rolls arrange themselves naturally with their axis, whenever possible, perpendicular to the lateral boundary [21]. Indeed, Schaeffer et al. [11] showed that the natural convection tends to increase maximum saturation. This is due to the fact that the Rayleigh–Bénard cells move the nucleation plane towards the upper plate. As a consequence a horizontal plane of supersaturation

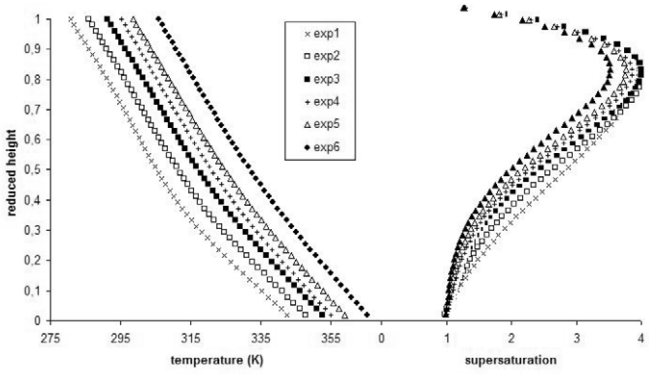

Fig. 3. Temperature and supersaturation profiles in the center of a TDCC.

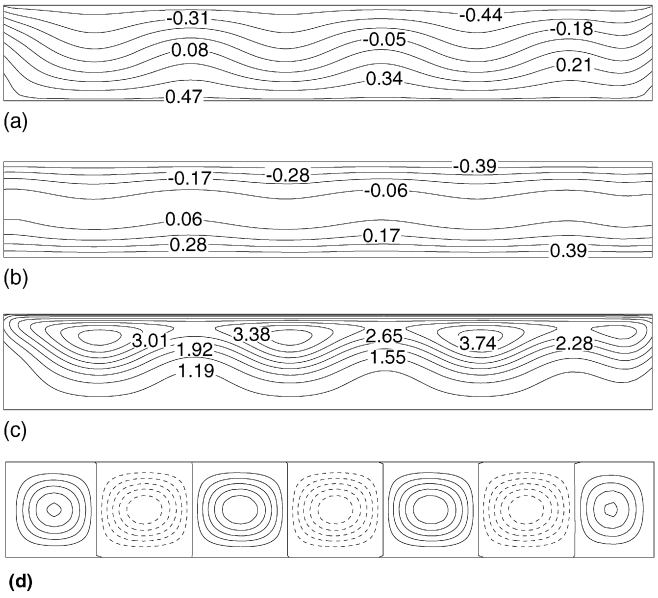

Fig. 4. Isolines corresponding to experiment 5 of Ref. [4] for (a) non-dimensional temperature, (b) non-dimensional mass fraction, (c) supersaturation, (d) stream function (15 isolines from −1.2 to 1.2 in steps of 0.2).

is not observed anymore. Accumulation of supersaturation zones tends to form in the downward region between pairs of convective cells (Fig. 4c). In the accumulation regions between two counter-rotating Bénard cells, the supersaturation can reach values greater than ones observed in conductive regime according to the Rayleigh number.

Finally, Table 4 gathers the numerical results obtained by the 2D model in the case of water/helium mixture. The average deviation of the supersaturation maximum between the numerical values with natural convection and the Heist and Reiss values is at most 35%. We have also reported in Fig. 2 the critical supersaturation data with respect to the temperature provided by our numerical approach (open triangles). The supersaturation predictions as obtained when convective contribution is accounted for in the TDCC, deviate significantly from data provided by Heist and Reiss [4] and as a consequence the observed numerical results are higher than those given by the Wölk et al. [7] correction.

In order to understand this large deviation, the methodology used by Heist and Reiss is briefly described. Firstly the temperature on the lower and upper plates and the pressure in the chamber are measured. Then, from these experimental data the partial pressure and temperature profiles and thus the saturation were calculated using a 1D model. In our study, using a 2D model, the profile of temperature obtained is not linear and consequently the values of

Table 4
Comparison of maximum saturations obtained from experiments and numerical calculations in convective regime for water in helium.

	Experimental maximum saturation	Numerical maximum saturation
Exp 1	3.59	4.40
Exp 2	3.44	4.56
Exp 3	3.26	4.41
Exp 4	3.05	4.22
Exp 5	2.96	4.11
Exp 6	2.70	3.83

S_{max} deviate approximately at most 35% from those obtained by Heist and Reiss. Note that, if the saturation value is compared in the center of the chamber (see Fig. 3) the deviation obtained is only of 15%.

4. Conclusion

In this work, a two-dimensional mass, momentum, energy equations written by considering the Boussinesq approximation have been numerically solved for describing the operating conditions in a thermal diffusion cloud chamber (TDCC). The model was compared with theoretical and experimental data of water droplets in binary gaseous mixture of water–helium.

Two simulation sets are made:

- The first simulation is carried out when the heat and mass transfer occur by diffusion only. The 2D model (neglecting convective fluxes and wall heating) has been tested by comparing its results with those by using a traditional 1D modeling of mass and heat transport process performed by Heist and Reiss. Consequently an agreement between numerical and experimental data was found.
- The second simulation is performed accounting for the convective contribution within the TDCC. Indeed, the effect of wall heating on the resulting profiles of temperature, saturation ratio and nucleation rate were found to be important particularly for operating conditions in which the heat and mass transfer within the TDCC is largely dominated by buoyancy-driven convective motion. Such fluid motions produce changes in the shape of temperature, mass fraction, supersaturation and nucleation rate profiles. As a consequence, the numerical results of the critical supersaturation were observed higher than the experimental data calculated by Heist and Reiss [4]. As a consequence, the empirical correction of nucleation rate developed by Wölk et al. [7] deviates significantly from 2D model results.

It can be concluded that operating conditions within TDCCs usually represent a fully two-dimensional problem and consequently the application of an inappropriate one-dimensional model can alter the results and yield a misleading rendering of the experimental results.

Acknowledgements

The authors are very grateful to Pr. Ph. Mirabel (University Louis Pasteur, Strasbourg, France) for helpful discussions.

References

[1] C.R.T. Wilson, Condensation of water vapor in the presence of dust-free air and other gases, Philos. Trans. R. Soc. London, Ser. A 189 (1897) 265.
[2] M. Volmer, H.Z. Flood, Tröpfchenbildung in Dämpfen, Zeitschrift für Physikalische Chemie 190 (1934) 273–285.
[3] J.L. Katz, B.J. Ostermier, Diffusion cloud-chamber investigation of homogeneous nucleation, J. Chem. Phys. 47 (2) (1967) 478–487.
[4] R.H. Heist, H. Reiss, Investigation of the homogeneous nucleation of water vapor using a diffusion cloud chamber, J. Chem. Phys. 59 (2) (1973) 665–671.
[5] Y. Viisanen, R. Strey, H. Reiss, Homogeneous nucleation rates for water, J. Chem. Phys. 99 (1993) 4680–4692.
[6] J. Wölk, R. Strey, Homogeneous nucleation of H2O and D2O in comparison: The isotope effect, J. Phys. Chem. B 105 (2001) 11683–11701.
[7] J. Wölk, R. Strey, C.H. Heath, B.E. Wyslouzil, Empirical function for homogeneous water nucleation rates, J. Chem. Phys. 117 (10) (2002) 4954–4960.
[8] R.H. Heist, M. Janjua, J. Ahmed, Effects of background gases on the homogeneous nucleation of vapors. 1, J. Chem. Phys. 98 (1994) 4443–4453.
[9] R.H. Heist, J. Ahmed, M. Janjua, Effects of background gases on the homogeneous nucleation of vapors. 2, J. Chem. Phys. 99 (1995) 375–383.
[10] F.T. Ferguson, J.A. Nuth III, The influence of buoyant convection on the operation of the upward thermal diffusion cloud nucleation chamber, J. Chem. Phys. 111 (17) (1999) 8013–8021.
[11] N. Schaeffer, F. Utheza, F. Garnier, G. Lauriat, Stable stratification alteration in a thermal cloud chamber, J. Chem. Phys. 113 (2000) 8085–8092.
[12] F.T. Ferguson, R.H. Heist, J.A. Nuth III, The effect of carrier gas pressure and wall heating on the operation of the thermal diffusion cloud chamber, J. Chem. Phys. 115 (23) (2001) 10829–10836.
[13] F. Stratmann, M. Wilck, V. Zdimal, J. Smolik, 2-D model for description of thermal diffusion cloud chambers: Description and first results, J. Phys. Chem. B 105 (2001) 11641–11648.
[14] Q. Wang, H. Yoo, Y. Jaluria, Convection in a horizontal rectangular duct under constant and variable property formulations, Int. J. Heat Mass Transfer 46 (2003) 297–310.
[15] R. Becker, W. Döring, Kinetissche Behandlung der Keimbildung in übersättigten Dämpfen, Ann. Physics 24 (1935) 719.
[16] D.C. Marvin, H. Reiss, Cloud chamber study of the gas phase photo-oxidation of sulfur dioxide, J. Chem. Phys. 69 (1978) 1897–1918.
[17] S. Patankar, Numerical Heat Transfer and Fluid Flow, Hemisphere, Washington, DC, 1980.
[18] C. Beghein, F. Haghighat, F. Allard, Numerical study of double-diffusive natural convection in a square cavity, Int. J. Heat Mass Transfer 35 (4) (1992) 833–846.
[19] A. Bertelsmann, R.H. Heist, Two-dimensional transport and wall effects in the thermal diffusion cloud chamber. I. Analysis and operations criteria, J. Chem. Phys. 106 (1997) 610–634.
[20] M. Velarde, C. Normand, La convection, Pour la science 35 (1980) 54.
[21] J.K. Platten, J.C. Legros, Convection in Liquids, Springer, Berlin, 1984.